Thermal demagnetization due to spin-wave and Stoner single-particle excitations in amorphous $Co_{90}Zr_{10}$ alloy

1992 J. Phys.: Condens. Matter 4 6429

(http://iopscience.iop.org/0953-8984/4/30/009)

J. Phys.: Condens. Matter 4 (1992) 6429–6442. Printed in the UK

Thermal demagnetization due to spin-wave and Stoner single-particle excitations in amorphous $Co_{90}Zr_{10}$ alloy

S N Kaul and P D Babu

School of Physics, University of Hyderabad, Central University PO, Hyderabad 500134, Andhra Pradesh, India

Received 15 March 1992

Abstract. Results of the high-precision magnetization (M) measurements performed on amorphous $Co_{90}Zr_{10}$ alloy at temperatures (T) ranging from 4.2 to 300 K in external magnetic fields (H) up to 15 kOe are presented. At low temperatures, magnetization does not saturate even at the highest field $H = 15$ kOe and the high-field differential susceptibility, $\chi_{hf}(0)$, is larger by an order of magnitude in the alloy in question than in crystalline Co. $M^2(H,T)$ versus $H/M(H,T)$ isotherms (Arrott plot isotherms) are nothing but a set of parallel straight lines at *high* fields ($H \gtrsim 3$ kOe) over the temperature range investigated. An elaborate analysis of the 'in-field', $M(H,T)$, as well as 'zero-field' (spontaneous), $M(0,T)$, magnetization data reveals that: (i) spin-wave excitations give a dominant contribution to thermal demagnetization of $M(0,T)$ for $T \lesssim 0.1T_c$ whereas Stoner single-particle excitations are mainly responsible for the decline of $M(0,T)$ with increasing temperature for $T \gtrsim 0.1T_c$; (ii) the particle–hole pair excitations are very *weakly* correlated; (iii) the spin-wave stiffness coefficient, D, is *independent* of H, *renormalizes with temperature* in accordance with the expression predicted by the itinerant-electron model and the D/T_c ratio possesses a value $\simeq 0.24$ meV Å^2 K^{-1} typical of Co-based amorphous alloys; and (iv) Stoner's criterion $IN(E_F) > 1$ for the occurrence of ferromagnetism is satisfied. The unusually large value of $\chi_{hf}(0)$, linear Arrott plot isotherms at high fields and the above features (i)–(iv) of the magnetization data find a straightforward explanation in terms of a theory proposed for weak itinerant ferromagnets.

1. Introduction

Amorphous (a-)$Co_{90}Zr_{10}$ happens to be one of the relatively well studied compositions in the a-$(Fe,Co,Ni)_{90}Zr_{10}$ alloy series and yet the nature of magnetism in this glassy alloy is far from being completely understood. To elucidate this point further, a-$Co_{90}Zr_{10}$ has been regarded as a *strong* itinerant-electron ferromagnet based on the recent low-temperature specific heat data [1] whereas the results of the early bulk magnetization (BM) measurements [2] provide strong evidence for *weak* itinerant-electron ferromagnetism in this alloy. Moreover, no definite conclusions about the existence of spin-wave excitations at low temperatures could be drawn from the BM data [2]. It was immediately recognized [2, 3] that the spontaneous magnetization, $M(0,T)$, must be determined to a far greater accuracy than that achieved hitherto if an unambiguous separation of the spin-wave and single-particle contributions to the thermal demagnetization of $M(0,T)$ was to be accomplished. Highly accurate (accuracy an order of magnitude higher than achieved previously [2]) BM measurements on a well characterized a-$Co_{90}Zr_{10}$ sample were undertaken in the temperature

0953-8984/92/306429+14$04.50

range 4.2 K $\leqslant T \leqslant$ 300 K with a view to resolving the controversy surrounding the nature of magnetism (*weak* versus *strong* itinerant ferromagnetism) and conclusively to support or rule out the presence of spin-wave excitations in this non-crystalline material at low temperatures.

2. Experimental details

Amorphous $Co_{90}Zr_{10}$ alloy was prepared in the form of ribbons ($\simeq$ 2 mm wide and $\simeq$ 0.03 mm thick) under inert (helium gas) atmosphere by the single-roller melt quenching technique. The amorphous nature of the fabricated ribbons was first verified by the x-ray diffraction method using Mo Kα radiation and then confirmed by the high-resolution electron microscopic (HREM) technique. The ribbons that did not reveal any crystalline regions upon HREM examination were used for the present magnetization studies. Magnetization (M) of the 'as-quenched' alloy ribbons was measured as a function of temperature (T) to a relative accuracy of better than 10 ppm (which is at least one order of magnitude higher than that achieved previously [2]) in the temperature range 4.2 to 300 K at various constant values of the applied magnetic field (H) in the interval 5 kOe $\leqslant H \leqslant$ 15 kOe by using the Faraday method while the sample was either cooled or heated at a rate of $\simeq$ 0.5 K min^{-1}. Also M was measured as a function of H in fields up to 15 kOe (the upper instrumental limit) at nearly 5 K intervals from 4.2 to 300 K by means of a vibrating sample magnetometer while the sample temperature was held constant to within $\pm$50 mK at a given temperature setting. In all the measurements, H was applied along the length within the ribbon plane in order to minimize the demagnetizing effects. We did not venture to extend these measurements to temperatures well above 300 K lest the actual magnetic behaviour was falsified by structural relaxation.

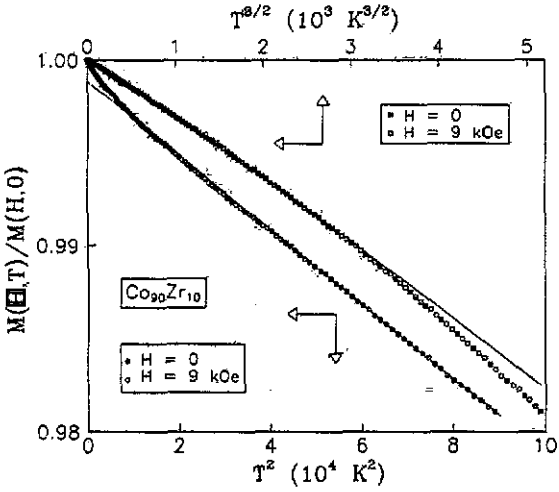

Figure 1. Normalized magnetization plotted against temperature in the form $[M(H,T)/M(H,0)]$ versus $T^{3/2}$ and $[M(H,T)/M(H,0)]$ versus T^2 at H = 0 and 9 kOe. The full curve and the straight line drawn through the data points represent the least-squares fits based on equations (9) and (11) of the text.

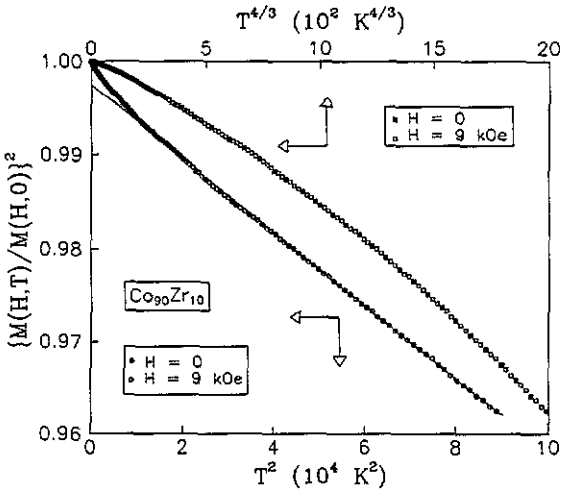

Figure 2. Plots of $[M(H,T)/M(H,0)]^2$ against T^2 and $T^{4/3}$ at $H = 0$ and 9 kOe. The straight line drawn through the data points denotes the least-squares fit based on equation (10) of the text.

3. Results and analysis

In order to find out the exact functional dependence of the 'in-field' magnetization, $M(H,T)$, on temperature, the reduced magnetization, $M(H,T)/M(H,0)$, is plotted against T^2 and $T^{3/2}$ in figure 1 whereas the reduced magnetization squared, $[M(H,T)/M(H,0)]^2$, is plotted against T^2 and $T^{4/3}$ in figure 2. It is noticed from these figures that $[M(H,T)/M(H,0)] \simeq 1 - BT^{3/2}$ for $T \lesssim 125$ K while the functional forms $[M(H,T)/M(H,0)]^2 \simeq 1 - AT^2$, and $[M(H,T)/M(H,0)] \simeq 1 - A'T^2$ seem to fit the observed temperature variation equally well in the temperature range 150 K $\lesssim T \leqslant 300$ K. The latter result is not surprising in view of the fact that the coefficient A is so small as to make the term $AT^2 \ll 1$ (as we shall show below) and the expression $[M(H,T)/M(H,0)]^2 = 1 - AT^2$ reduces to $[M(H,T)/M(H,0)] \simeq 1 - A'T^2$ with $A' = A/2$. The above findings, i.e. $M(H,T)$ varies as $T^{3/2}$ for $T \lesssim 125$ K and as T^2 for higher temperatures, assert that the observed temperature dependence of the relative deviation of magnetization from its value at 0 K (no distinction between the values of M at 4.2 K and 0 K is made in this work), i.e. $[M(H,0) - M(H,T)]/M(H,0) \equiv \Delta m(T)$, should be analysed in terms of the expression

$$\Delta m(T) = \Delta m_{sw}(T) + \Delta m_{sp}(T) \tag{1}$$

where the spin-wave, Δm_{sw}, and single-particle, Δm_{sp}, contributions to Δm are given by [4, 5]

$$\Delta m_{sw} = \frac{g\mu_B}{M(H,0)}\left[Z\left(\tfrac{3}{2},t_H\right)\left(\frac{k_B T}{4\pi D(T)}\right)^{3/2} + 15\pi\beta Z\left(\tfrac{5}{2},t_H\right)\left(\frac{k_B T}{4\pi D(T)}\right)^{5/2}\right] \tag{2}$$

and

$$\Delta m_{sp}(T) = \begin{cases} A'(H)T^{3/2}\exp(-\Delta/k_B T) & \text{for a } \textit{strong} \text{ itinerant ferromagnet} \quad (3a) \\ A'(H)T^2 & \text{for a } \textit{weak} \text{ itinerant ferromagnet.} \quad (3b) \end{cases}$$

In equation (2), the Bose–Einstein integral functions

$$Z(s,t_H) = \xi(s)F(s,t_H) = \sum_{n=1}^{\infty} n^{-s}\exp(-nt_H) \tag{4a}$$

with

$$t_H = T_g/T = g\mu_B H_{eff}/k_B T \tag{4b}$$

allow for the extra energy gap, $g\mu_B H_{eff}\,(= k_B T_g)$, in the spin-wave spectrum arising from the effective field

$$H_{eff} = H - 4\pi NM + H_A \tag{5}$$

where N, M and H_A are the demagnetizing factor, magnetization and anisotropy field, respectively. Alternatively, in the presence of the external magnetic field, H, the magnon dispersion relation takes the form

$$E_q(T) = \hbar\omega_q(T) = g\mu_B H_{eff} + D(T)q^2(1 - \beta q^2) \tag{6}$$

where the coefficient β is related to the mean-square range of the exchange interactions, $\langle r^2\rangle$, as $\langle r^2\rangle = 20\beta$ and the spin-wave stiffness coefficient, D, renormalizes with temperature according to the relations [4–7]

$$D(T) = D_0(1 - D_2T^2) \tag{7a}$$

and

$$D(T) = D_0(1 - D_{5/2}T^{5/2}) \tag{7b}$$

for the itinerant- and localized-electron models, respectively. Having determined the demagnetizing factor N from the low-field magnetization measurements and the splitting factor $g = 2.09 \pm 0.02$ (note that this value is in better agreement with the value $g = 2.06 \pm 0.03$ previously reported [8] for FCC Co than with the numerical estimate of $g = 2.18 \pm 0.02$ quoted [9] for HCP Co) and anisotropy field H_A from ferromagnetic resonance measurements [10], theoretical fits to the Δm_H data have been attempted based on equations (1)–(5) with $D(T)$ in equation (2) given by either equation (7*a*) or (7*b*). When the least-squares fit involving six parameters, i.e. $M(H,0)$, D_0, D_2 or $D_{5/2}$, β, A' and Δ, yielded the result $\Delta/k_B = 0 \pm 1$ K, equations (1), (2) and (3*b*) involving the combinations $D(T) = D_0$, $D(T) = D_0(1 - D_2T^2)$ and $D(T) = D_0(1 - D_{5/2}T^{5/2})$ with either $\beta = A' = 0$ or $\beta = 0$, $A' \neq 0$ or $\beta \neq 0$, $A' = 0$ were used for the subsequent fits. In order to ascertain the relative importance of the spin-wave and single-particle contributions to Δm within the temperature range covered in the present experiments, a 'range-of-fit' analysis has been carried out in which the values of *free* fitting parameters in the above-mentioned theoretical fits are monitored as the temperature interval $T_{min} \leqslant T \leqslant T_{max}$ is progressively broadened by keeping T_{min} fixed at 4.2 K and varying T_{max} from 28 to 300 K. The results of this analysis are depicted in figure 3.

In these plots, we define a *reduced* sum of deviation squares χ_r^2 as χ^2 for the $M(H,T)$ data in a given temperature interval divided by the total number of data points (N) in that interval minus the number of free fitting parameters (N_{para}), i.e. $\chi_r^2 = \chi^2/(N - N_{para})$, so as to make comparison between the parameter values

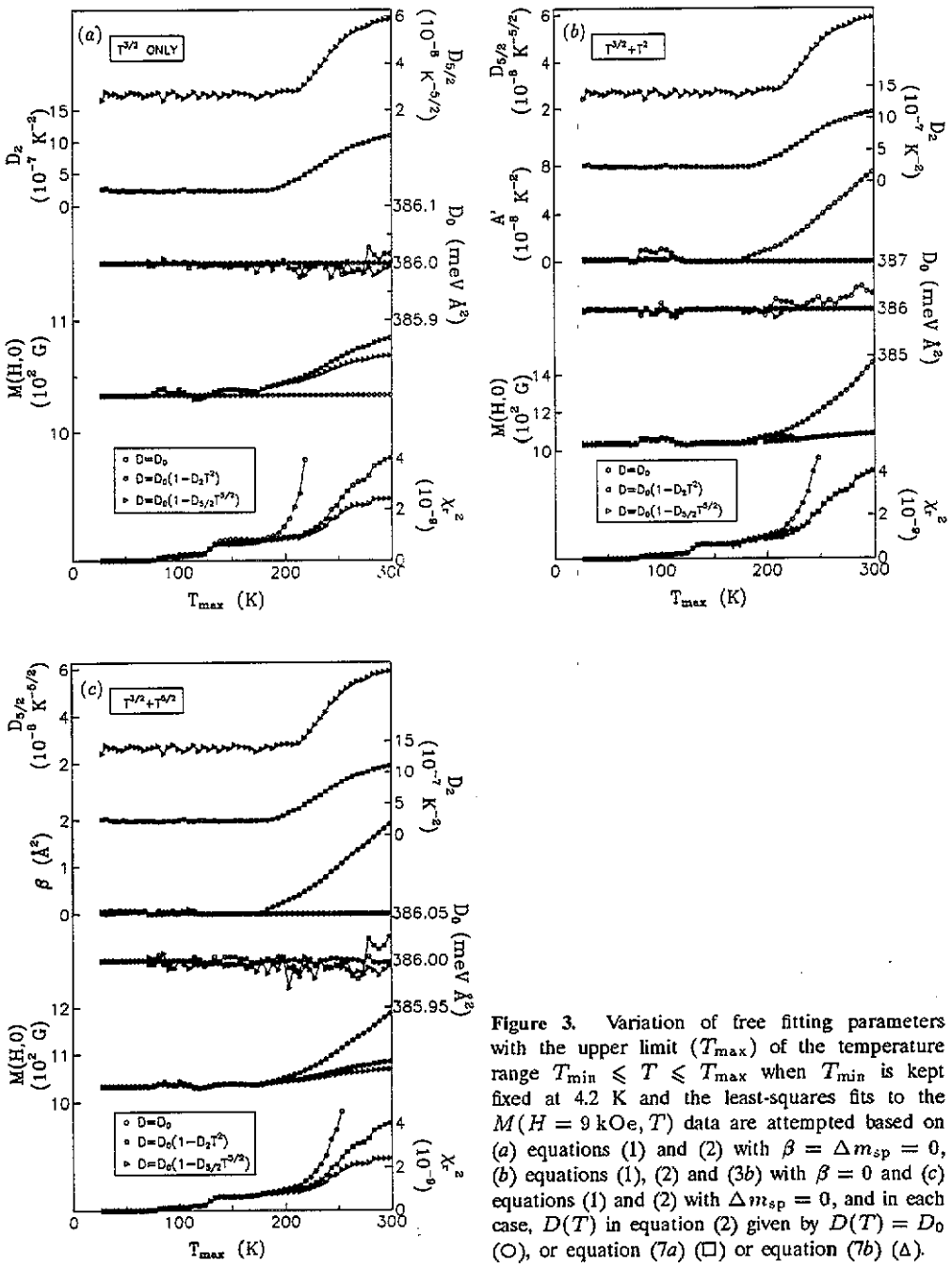

Figure 3. Variation of free fitting parameters with the upper limit (T_{max}) of the temperature range $T_{min} \leqslant T \leqslant T_{max}$ when T_{min} is kept fixed at 4.2 K and the least-squares fits to the $M(H = 9\,kOe, T)$ data are attempted based on (*a*) equations (1) and (2) with $\beta = \Delta m_{sp} = 0$, (*b*) equations (1), (2) and (3*b*) with $\beta = 0$ and (*c*) equations (1) and (2) with $\Delta m_{sp} = 0$, and in each case, $D(T)$ in equation (2) given by $D(T) = D_0$ (○), or equation (7*a*) (□) or equation (7*b*) (△).

obtained in different temperature intervals physically meaningful and to be able to assess the quality of such fits as a function of T_{max}. Judging by the value of χ_r^2 and by the stability of the fitting parameters against a wide variation in T_{max}, the following observations can be made from the data presented in figure 3. (i) Out of

all the fits attempted, the one based on the theoretical expression that combines equations (1), (2) and (7*a*) and sets $\Delta m_{sp} = \beta = 0$ reproduces the observed temperature dependence of Δm with the greatest accuracy for $T \lesssim 170$ K (this result is at variance with our earlier finding [2] that Δm_{sp} completely accounts for Δm in the entire temperature range from 4.2 to 300 K). But for temperatures above 170 K even this combination, like other combinations, fails to provide an adequate description for the observed variation of Δm with T in that most of the fitting parameters, including χ_r^2, exhibit unphysical increase with T_{max}. (ii) Regardless of the temperature range chosen for the fit, inclusion of the single-particle contribution (the T^2 term) or the higher-order spin-wave term (the $T^{5/2}$ term) beside the $T^{3/2}$ term in equations (1) and (2) leaves values for the parameters of the $T^{3/2}$ fit (i.e. the fit that makes use of equations (1) and (2) with $\Delta m_{sp} = \beta = 0$) practically unaltered and does not bring forth any improvement in the quality of the fit. On the contrary, χ_r^2 assumes a slightly higher value and the additional parameter (i.e. A' in the former case and β in the latter) possesses negligibly small value. (iii) The quality of the least-squares fits to Δm data based on the theoretical expressions that set $D(T) = D_0$ is *much* worse compared with those that allow D to vary with T in accordance with either equation (7*a*) or (7*b*). (iv) The functional dependence of D on T for $T \lesssim 170$ K is better described by equation (7*a*) than by (7*b*) as inferred from the value of χ_r^2, which is consistently lower for the fits that employ equation (7*a*) than for those that use equation (7*b*). For the sake of completeness, the Δm data have also been fitted to equation (1) with $\Delta m_{sw} = 0$ and Δm_{sp} given by equation (3*a*) or (3*b*), with the result that equation (3*b*) yields a variation of Δm with T in close agreement with the experimentally observed one only in the temperature interval 220 K $\lesssim T \leqslant 300$ K whereas the theoretical variation predicted by equation (3*a*) does not bear any resemblance whatsoever to that observed within the specified temperature range even with unphysical values for the parameters A' and Δ. The lower limit $T^* \simeq 220$ K for the temperature range over which equation (3*b*) or its more general form, i.e.

$$[M(H,T)/M(H,0)] = C' - A'T^2 \tag{8a}$$

adequately describes the temperature dependence of Δm is determined from the 'range-of-fit' analysis, in which T_{max} is kept fixed at 300 K and T_{min} is progressively lowered towards 4.2 K, by identifying T^* with the temperature at which χ_r^2 goes through a *minimum* as a function of T_{min} (figure 4(*b*)). Having determined T^* in this way, the optimum values for the fitting parameters are obtained by monitoring them as a function of T_{max} (as was done previously) in the 'range-of-fit' analysis wherein T_{min} is held constant at T^* and T_{max} is raised towards 300 K (figure 4(*a*)). Finally, we made an attempt to fit the Δm data to the empirical expression, i.e.

$$[M(H,T)/M(H,0)]^2 = C - 2AT^2 \tag{8b}$$

suggested by the plots shown in figure 2, using the 'range-of-fit' analysis of the type just mentioned in connection with equation (3*b*) or (8*a*). The results of this analysis are also included in figure 4. It is evident from the data presented in figure 4 that equation (8*b*) provides a better fit to the $\Delta m(T)$ data over a wider temperature range than equation (3*b*) or (8*a*) does. Note that in figure 4 χ_r^2 values for the fits based on equations (8*a*) and (8*b*) are calculated for the data in the form $M(H,T)/M(H,0) = 1 - \Delta m(T)$ with a view to ascertaining which of the fits is better.

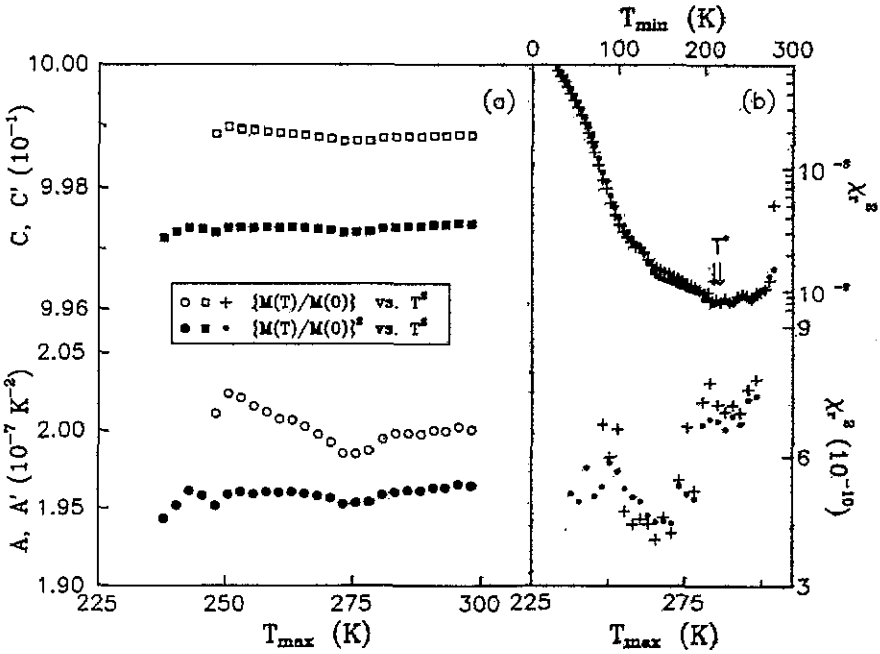

Figure 4. (*a*) Variation of free fitting parameters with the upper limit (T_{max}) of the temperature range $T_{min} \leqslant T \leqslant T_{max}$ when T_{min} is kept fixed at T^* and the least-squares fits to the $M(H,T)$ data taken at $H = 0$ and 9 kOe are attempted based on equations (8*a*) (open symbols) and (8*b*) (full symbols). (*b*) Variation of χ_r^2 with the lower limit T_{min} (upper limit T_{max}) of the temperature range $T_{min} \leqslant T \leqslant T_{max}$ when T_{max} (T_{min}) is held constant at 300 K (T^*) and the least-squares fits to the $M(H,T)$ data taken at $H = 0$ and 9 kOe are attempted based on equations (8*a*) (+) and (8*b*) (●).

The magnetization data taken at other fixed values of the external magnetic field have been analysed the same way as mentioned above for the $M(H,T)$ data taken at $H = 9$ kOe. Such an elaborate data analysis reveals that

$$\Delta m(T) = [g\mu_B/M(H,0)]Z(\tfrac{3}{2},t_H)[k_B T/4\pi D_0(1 - D_2T^2)]^{3/2} \quad (9)$$

for $0 \lesssim T \lesssim 175$ K with $g = 2.09 \pm 0.02$ [10], $D_0 = 386 \pm 4$ meV Å^2, $D_2 = (2.58 \pm 0.32) \times 10^{-7}$ K^{-2}, $M(H,0) = 1033.56$ G at $H = 9$ kOe,

$$[M(H,T)/M(H,0)]^2 = (0.9973 \pm 0.0002) - 2(1.95 \pm 0.01) \times 10^{-7}T^2 \quad (10)$$

for 210 K $\lesssim T \leqslant 300$ K and

$$[M(H,T)/M(H,0)] = (0.9988 \pm 0.0001) - (2.005 \pm 0.020) \times 10^{-7}T^2 \quad (11)$$

for 220 K $\lesssim T \lesssim 300$ K. In equations (9)–(11), all the parameters with the exception of $M(H,0)$ and $Z(\frac{3}{2},t_H)$ are *independent* of the external field H. The least-squares fits (9)–(11) are represented by the straight lines (curves) drawn through the data points in figures 1 and 2.

Figure 5 shows $M^2(H,T)$ plotted against $H/M(H,T)$ at a few representative but fixed temperature values in the range 4.2 to 300 K. In accordance with our earlier findings [2]: (i) the magnetization does not saturate even in fields as high as

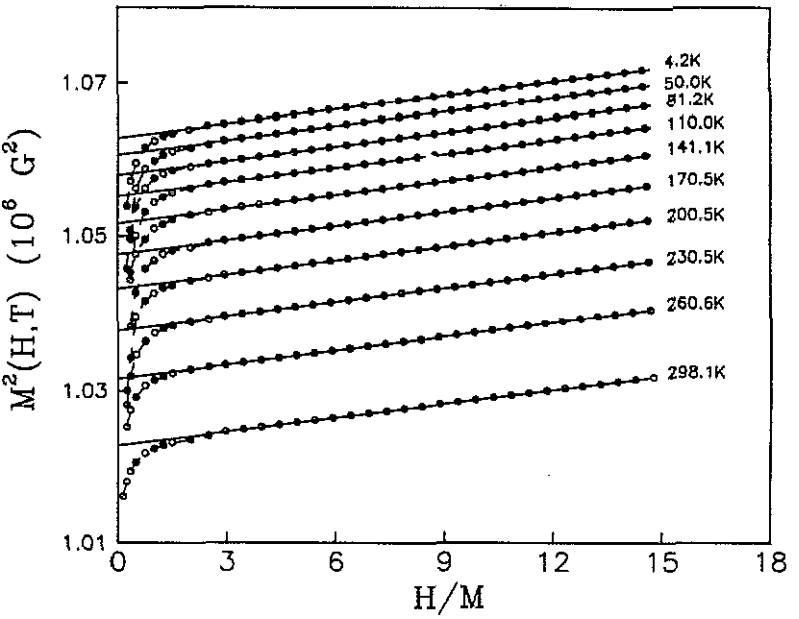

Figure 5. $M^2(H,T)$ versus $H/M(H,T)$ isotherms at a few representative temperatures.

15 kOe at low temperatures; (ii) the high-field susceptibility, χ_{hf}, has a *temperature-independent* value of $(3.5 \pm 0.5) \times 10^{-5}$ emu g^{-1} Oe^{-1} within the temperature range 4.2 K $\leqslant T \leqslant$ 300 K, and is an order of magnitude larger [11] in this glassy alloy† than in crystalline Co; and (iii) the Arrott plot (M^2 versus H/M) isotherms are nothing but a set of parallel straight lines for fields $H \gtrsim 3$ kOe and for all temperatures $\leqslant$ 300 K. Accurate values of the spontaneous magnetization at different temperatures, $M(0,T)$, are determined from the intercepts $M^2(0,T)$ on the ordinate of the M^2 versus H/M plot (figure 5) by a linear extrapolation of the straight-line isotherms to $(H/M) = 0$. The $M(0,T)$ data so obtained are used to construct $[M(0,T)/M(0,0)]$ versus T^2 and $T^{3/2}$ and $[M(0,T)/M(0,0)]^2$ versus T^2 and $T^{4/3}$ plots shown in figures 1 and 2 with a view to ascertaining the exact functional form of $M(0,T)$. It is evident from the data presented in these figures that $M(0,T)$ follows the *same* temperature dependence as $M(H,T)$ does. Thus, equations (9) and (10) with $M(H,T)$, $M(H,0)$ and $Z(\frac{3}{2}, t_H)$ replaced by $M(0,T)$, $M(0,0)$ $(= 1030.91\,\mathrm{G})$ and $\xi(\frac{3}{2})$, respectively, provide the best least-squares theoretical fit to the $M(0,T)$ data too. The presently determined value of the spin-wave stiffness coefficient $D = 386 \pm 4$ meV Å^2 compares favourably with the value $D_m = 370$ meV Å^2 quoted by Kanemaki *et al* [12] for a-$Co_{90}Zr_{10}$ based on magnetization measurements and is in much better agreement with the inelastic neutron scattering (INS) estimate of $D_n = 385$ meV Å^2 for FCC $Co_{94}Fe_6$ [13] or $D_n = 380$ meV Å^2 for FCC $Co_{92}Fe_8$ [14] than with the generally accepted [11] INS value $D_n = 510$ meV Å^2 for HCP Co. Furthermore, the values of $M(0,0)$ and

† Admittedly, the highest value of the magnetic field used in the present measurements is not intense enough to yield an accurate estimate of the high-field susceptibility, χ_{hf}. Nevertheless, χ_{hf} for other crystalline or amorphous ferromagnets evaluated in a field range comparable to that used in the present case undoubtedly has a much smaller value than that for the glassy alloy in question.

$M(H,0)$ obtained from the least-squares fits exactly match with those (within 0.1%) measured at 4.2 K and the magnetic moment per Co atom at 4.2 K, $\mu_{Co} = 1.52\mu_B$, conforms well with the value $1.56\,\mu_B$ for FCC Co [15] but not with that ($1.71\,\mu_B$) reported [11] for HCP Co.

4. Discussion

Before embarking upon a discussion of the results, we briefly summarize the main findings. (i) Magnetization does not saturate in fields up to 15 kOe at low temperatures and high-field susceptibility is *independent* of temperature in the entire temperature range covered in the present experiments. (ii) $M^2(H,T)$ versus $H/M(H,T)$ isotherms are *linear* over a wide range of temperatures particularly at high fields (these isotherms exhibit a marked curvature at low fields). (iii) The spontaneous magnetization, $M(0,T)$, varies with temperature as

$$[M(0,T)/M(0,0)] = 1 - BT^{3/2} \tag{12}$$

for $T \lesssim 175$ K and

$$[M(0,T)/M(0,0)]^2 = 1 - 2AT^2 \tag{13}$$

for $210\ \text{K} \lesssim T \leqslant 300$ K with $A = (1.95 \pm 0.01) \times 10^{-7}\ \text{K}^{-2}$.

Though the theory, based on the Stoner model, proposed by Edwards and Wohlfarth (EW) [16] for weak itinerant ferromagnets is capable of explaining *qualitatively* the observations (i) and (ii) mentioned above, EW theory cannot account for observation (iii) because it asserts that $[M(0,T)/M(0,0)]^2 \propto T^2$ (equation (13)) at all temperatures $T \ll T_F$ (the effective Fermi degeneracy temperature) and invariably overestimates T_c. As a consequence of the latter limitation, this theory yields a value for the coefficient A in equation (13) which is an order of magnitude smaller than that actually observed. Of all the theoretical treatments [17–22] that overcome the major deficiencies (failure to predict the Curie temperature correctly and to explain the Curie–Weiss behaviour of magnetic susceptibility for $T > T_c$) in the conventional Stoner model, only the one [20] that includes the corrections to the Stoner model arising from the *transverse* as well as *longitudinal local* spin-density fluctuations and incorporates a natural temperature-dependent cut-off wavevector for the thermally excited modes offers a straightforward explanation for all three observations, as shown below. This theory, due to Lonzarich and Taillefer (LT) [20], yields a magnetic equation of state, valid at high fields only, for weak itinerant ferromagnets of the form

$$H = a(T)M(H,T) + bM^3(H,T) \tag{14}$$

with

$$a(T) = -[2\chi(0,0)]^{-1}[1 - (T/T_c)^2] \tag{15}$$

$$b^{-1} = 2\chi(0,0)M^2(0,0) \tag{16}$$

where

$$\chi(0,0) = N\mu_B^2 N(E_F)(T_F/T_c)^2 = N\mu_B^2 N(E_F)S \tag{17}$$

$$M^2(0,0) = (N\mu_B\mu)^2 = (S\gamma)^{-1} \tag{18}$$

$$T_F^{-2} = (\pi^2 k_B^2/6)\nu \tag{19}$$

$$\nu = [N'(E_F)/N(E_F)]^2 - [N''(E_F)/N(E_F)] \tag{20}$$

$$S = [IN(E_F) - 1]^{-1} \tag{21}$$

$$\gamma = \{8N^2\mu_B^2[N(E_F)]^2\}^{-1}\{[N'(E_F)/N(E_F)]^2 - [N''(E_F)/3N(E_F)]\}. \tag{22}$$

In equations (15)–(22), $\chi(0,0)$ and μ are the zero-field differential susceptibility and moment per alloy atom at 0 K, respectively, S is the Stoner enhancement factor, I is a measure of the exchange interaction, N is the number of atoms per unit volume, $N(E_F)$ is the density of single-particle states at the Fermi level E_F, and $N'(E_F)$ ($N''(E_F)$) is its first (second) energy derivative. An expression for $M(0,T)$ valid over a wide range of intermediate temperatures and the same as equation (13) can be obtained from equation (14) by setting $H = 0$ in this equation and solving for $M(0,T)$. Depending on whether only equations (15) and (16) or whether equations (15)–(22) are used to substitute for the coefficients $a(T)$ and b in equation (14), two different expressions for the coefficient A in equation (13) are obtained, i.e.

$$A = (2T_c^2)^{-1} \tag{23}$$

$$A = \tfrac{1}{2}(2\pi k_B f/\mu)^2[N(E_F)]^2 \tag{24}$$

with

$$f^2 = \{[N'(E_F)/N(E_F)]^2 - [N''(E_F)/N(E_F)]\} / \{3[N'(E_F)/N(E_F)]^2 - [N''(E_F)/N(E_F)]\}. \tag{25}$$

While the properties (i) and (ii) are an immediate consequence of the form of equation (14), the temperature-independent nature of the coefficient b and weak field dependence of the coefficients a and b, the temperature variation of spontaneous magnetization of the type given by equation (13) follows from equation (14) as elucidated above. Moreover, the LT model, unlike the EW model, correctly predicts that $M(0,T) \propto T^{3/2}$ at low temperatures and $M^2(0,T) \propto T^{4/3}$ for temperatures close to T_c. Thus, within the framework of the LT model, the above observation (iii) (equations (12) and (13)) implies that the spin-wave excitations alone and the Stoner single-particle excitations as well as local spin-density fluctuations are responsible for the thermal demagnetization of spontaneous magnetization for $T \lesssim 175$ K and over the range 210 K $\lesssim T \lesssim$ 300 K, respectively. Considering the well known fact that the local spin-density fluctuations get strongly suppressed [7, 23] in the presence of an external magnetic field, the close agreement between the $M(0,T)$ and $M(H,T)$ data (figures 1 and 2) strongly suggests that the quadratic temperature variation of $[M(0,T)/M(0,0)]^2$ for $T \gtrsim 200$ K (equation (13)) should mainly arise from the Stoner single-particle excitations. Alternatively, the particle–hole pair excitations in a-$Co_{90}Zr_{10}$ are very *weakly correlated*. In such a case, the LT theory predicts that $M(0,T)$ should vary with T in accordance with equation (13) over a wide range

of temperatures extending up to T_c. A reliable estimate of T_c can, therefore, be obtained by substituting the presently determined value of A in equation (23). This procedure yields $T_c = 1605 \pm 5$ K, which conforms well not only with our earlier [2] estimate of 1615 ± 5 K and with the *extrapolated* value [24] of 1500 ± 100 K, arrived at by fitting a Brillouin function to the temperature dependence of magnetization exhibited by a-$Co_{90}Zr_{10}$ up to its crystalline temperature, but also with the value ($\simeq$ 1600 K) predicted by the recent theoretical calculations [25] (which take into account the *thermal* fluctuations in the *local* magnetic moment as well as the *local* spin-density fluctuations induced by the *structural disorder*) for *amorphous* Co with FCC-like atomic short-range order.

Equation (24) permits a calculation of $N(E_F)$ provided the exact value of the function f (equation (25)) is known; the values for the quantities μ and A have already been determined. This requires a complete knowledge about the actual shape of the density of states (DOS) curve (see equation (25)), which is lacking at present for the alloy in question. However, recent ultraviolet photoemission spectroscopic (UPS) studies [26] on a-$TM_{90}Zr_{10}$ (TM=Fe, Co, Ni, Cu) alloys show that the Fermi level in a-$Co_{90}Zr_{10}$ lies fairly close to the top of the narrow 3d band. If we assume that the 3d band is Gaussian-like in shape (which the UPS data [26] strongly indicate), $f \simeq 1$ (see the appendix). Setting $f = 1$ and using the presently determined values $A = (1.95 \pm 0.01) \times 10^{-7}\,K^{-2}$ and $\mu = 1.366\,\mu_B$ in equation (24) yields the value for the DOS at E_F as $N(E_F) = 1.58 \pm 0.01$ states eV^{-1} $atom^{-1}$. This value should be compared with the band-structure estimates 1.24 for HCP Co [27], 1.98 for FCC Co [28, 29], 1.17 for Co_3Zr [30] and 1.32 (the *local* $N(E_F)$ values at the Co and Zr sites given by Oelhafen [30] are weighted by the relative concentrations of Co and Zr in $Co_{90}Zr_{10}$ to arrive at this value) for crystalline $Co_{90}Zr_{10}$ alloy, and also with the values 1.73 ± 0.05 [31], 1.94 ± 0.02 [1] and 2.34 ± 0.01 [12] deduced from the recently measured [1, 12, 31] values of the coefficient $\gamma_E = (\pi^2 k_B^2/3) N(E_F)$ of the electronic specific heat for a-$Co_{90}Zr_{10}$ after making corrections [12] for the electron–phonon enhancement. (Note that all the values of $N(E_F)$ quoted above are in units of states eV^{-1} $atom^{-1}$.) Consistent with the *direct* structural evidence [32, 33] for an *FCC-like* short-range order in the glassy alloy in question and with the exact coincidence of the values of g, μ_{Co} and D for a-$Co_{90}Zr_{10}$ with those previously reported for FCC Co, the above comparison, apart from bringing out the fact that reasonably good agreement exists between the results of magnetization and low-temperature specific heat measurements (see appendix) considering the uncertainty in the determination of the function f which appears in equation (24), demonstrates that $N(E_F)$ has nearly the *same* value for both a-$Co_{90}Zr_{10}$ and FCC Co whereas the DOS at E_F in a-$Co_{90}Zr_{10}$ is much *higher* than that in HCP Co. In view of the well known fact that both spin-up and spin-down DOS contribute to $N(E_F)$ in the weak itinerant ferromagnet while $N(E_F) \simeq N_\downarrow(E_F)$ for a strong itinerant ferromagnet, the large *enhancement* in $N(E_F)$ for a-$Co_{90}Zr_{10}$ compared to the value of DOS in the HCP Co (a strong itinerant ferromagnet) is a direct consequence of weak itinerant ferromagnetism in a-$Co_{90}Zr_{10}$. Thus, contrary to the previous claim [1], this inference in conjunction with our earlier observations, i.e. larger high-field susceptibility at low temperatures, T^2 variation of $M(0, T)$ over a wide range of intermediate temperatures, etc., asserts that a-$Co_{90}Zr_{10}$ is a *weak* itinerant ferromagnet.

Having estimated T_c and $N(E_F)$ for a-$Co_{90}Zr_{10}$, a calculation of the exchange and band parameters is undertaken with a view to finding out how the calculated values compare with the corresponding values reported for other crystalline and

amorphous itinerant ferromagnets. First, the value $\chi(0,0) = (3.07 \pm 0.04) \times 10^{-4}$ for the 'zero-field' susceptibility at 4.2 K, $\chi(0,0)$, is calculated from the observed slope b^{-1} (equation (14)) of the $M^2(H,T)$ versus $H/M(H,T)$ isotherm at 4.2 K using equation (16). The values $T_c = 1605 \bullet 5$ K, $N(E_F) = 1.94 \pm 0.06$ states eV^{-1} $atom^{-1}$ (this seems to be the most reliable value considering the high quality of the specific heat data from which it is deduced) and the above value for $\chi(0,0)$ are then used in equations (17), (19), (20) and (21) to arrive at the numerical estimates $S = 36 \pm 4$, $IN(E_F) = 1.028 \pm 0.003$, $I = 0.53 \pm 0.06$ eV, $T_F = 9650 \pm 350$ K and $\nu = 0.9 \pm 0.1$ eV^{-2}. These values conform well with the corresponding values summarized earlier [2, 34] for a number of crystalline as well as amorphous weak itinerant ferromagnets. While the presently determined value of I is in consonance with the value $I = 0.49$ eV reported [28, 29] for FCC Co, the above estimate for $IN(E_F)$ shows that Stoner's criterion $IN(E_F) > 1$ for the occurrence of ferromagnetism is satisfied.

5. Summary and conclusions

An elaborate analysis of highly accurate magnetization data for the first time permits an unambiguous separation of spin-wave and single-particle contributions to thermal demagnetization in a-$Co_{90}Zr_{10}$ and enables us to draw the following conclusions.

Magnetization at 4.2 K does not saturate even for fields as high as 15 kOe; the high-field differential susceptibility, $\chi_{hf}(0)$, is larger by at least one order of magnitude in the glassy alloy in question than in crystalline Co.

$M^2(H,T)$ versus $H/M(H,T)$ isotherms are linear at *high* fields over the entire range of temperatures investigated. The slope of these straight-line isotherms is nearly *independent* of temperature within the interval $4.2\ \text{K} \leqslant T \leqslant 300$ K.

Spin-wave excitations give a dominant contribution to thermal demagnetization of spontaneous magnetization, $M(0,T)$, for temperatures $T \lesssim 0.1T_c$ whereas Stoner single-particle excitations are mainly responsible for the decline of $M(0,T)$ with increasing temperature for $T \gtrsim 0.1T_c$.

The particle–hole pair excitations are very *weakly correlated*.

The spin-wave stiffness coefficient, D, is *independent* of the external magnetic field and possesses a value close to that found in FCC Co. The D/T_c ratio, which is a measure of the range of the exchange interactions, has a value $\simeq 0.24$ meV $Å^2$ K^{-1}, typical of Co-containing crystalline and amorphous alloys.

The density of states at the Fermi level has as large a value as for FCC Co.

The above aspects of the magnetization data find a satisfactory explanation in terms of a theory proposed by Lonzarich and Taillefer for weak itinerant ferromagnets.

The Stoner criterion $IN(E_F) > 1$ for the occurrence of ferromagnetism is satisfied.

In conformity with the results of the structural studies, the present data provide ample experimental evidence for FCC-like short-range order in the glassy alloy in question.

Acknowledgments

The authors are grateful to the Department of Science and Technology, New Delhi, for financially supporting this work under project no. SP/S2/M21/86. One of us (PDB) is grateful to the University Grants Commission, New Delhi, for financial support.

Appendix

We assume that the peak in the density of states (DOS) curve near the Fermi energy, E_F, can be approximated by a Gaussian probability density function, i.e.

$$N(E) = (2\pi\sigma^2)^{-1/2} \exp\{-\tfrac{1}{2}[(E - \langle E\rangle)/\sigma]^2\} \tag{A1}$$

where the mean or average energy $\langle E\rangle = \int_{-\infty}^{\infty} EN(E)\,dE$ and the mean square deviation or variance $\sigma^2 = \int_{-\infty}^{\infty}(E - \langle E\rangle)^2 N(E)\,dE$ so that

$$N'(E_F) = (dN(E)/dE)|_{E=E_F} = N(E_F)(\langle E\rangle - E_F)/\sigma^2$$

or

$$N'(E_F)/N(E_F) = (\langle E\rangle - E_F)/\sigma^2 \tag{A2}$$

and

$$N''(E_F) = (d^2N(E)/dE^2)|_{E=E_F} = N'(E_F)(\langle E\rangle - E_F)/\sigma^2 - N(E_F)/\sigma^2$$

or

$$N''(E_F)/N(E_F) = [(\langle E\rangle - E_F)/\sigma^2]^2 - 1/\sigma^2. \tag{A3}$$

In arriving at equation (A3), use has been made of equation (A2). The band parameters ν, γ^* and f defined by equations (20), (22) and (25) of the text, respectively, can now be calculated using equations (A2) and (A3) as follows:

$$\nu = \{[N'(E_F)/N(E_F)]^2 - [N''(E_F)/N(E_F)]\} = 1/\sigma^2 \tag{A4}$$

$$\gamma^* = 24N^2\mu_B^2[N(E_F)]^2\gamma = \{3[N'(E_F)/N(E_F)]^2 - [N''(E_F)/N(E_F)]\}$$
$$= 2[(\langle E\rangle - E_F)/\sigma^2]^2 + 1/\sigma^2 \tag{A5}$$

$$f = (\nu/\gamma^*) = \{1 + 2[(\langle E\rangle - E_F)/\sigma]^2\}^{-1/2} \simeq 1 - [(\langle E\rangle - E_F)/\sigma]^2. \tag{A6}$$

It is evident from equation (A6) that $f = 1$ only when $E_F = \langle E\rangle$, i.e. when E_F denotes the energy corresponding to the top of the 3d band. Now that the present magnetization data give the value for ν as $\nu \simeq 1$ eV^{-2} (see the text), the variance σ^2, according to equation (A4), equals 1 eV^2 and equation (A6) reduces to

$$f \simeq 1 - (\langle E\rangle - E_F)^2. \tag{A7}$$

In order that the magnetization data yield the same value as that (1.94 states eV^{-1} $atom^{-1}$) obtained from the low-temperature specific heat data [1], the parameter f in equation (25) of the text should possess the value $\simeq 0.81$. In the light of equation (A7), this implies that the Fermi level should lie *below* the top of the 3d band (in consonance with the recent UPS studies [26] on a-$Co_{90}Zr_{10}$) and the energy difference between $E_{top} = \langle E\rangle$ and E_F should be $\simeq 0.436$ eV. Consistent with the observations made at various stages of the text, this value is close to that (0.4 eV) found [11] in FCC Co.

References

[1] Rosenberg M, Hardebusch U, Schöne-Warnefeld A, Wernhardt R and Fukamichi K 1988 *J. Phys. F: Met. Phys.* **118** 2259
[2] Kaul S N 1983 *Phys. Rev.* B **27** 6923
[3] Kaul S N 1984 *Solid State Commun.* **52** 1015
[4] Keffer F 1966 *Encyclopedia of Physics* ed H P J Wijn (Berlin: Springer) vol XVIII, part 2, p 1
[5] Mathon J and Wohlfarth E P 1968 *Proc. R. Soc.* A **302** 409
[6] Izuyama T and Kubo R 1964 *J. Appl. Phys.* **35** 1074
[7] Kaul S N 1991 *J. Phys.: Condens. Matter* **3** 4027
[8] Rodbell D S 1962 *J. Appl. Phys.* **33** 1126
[9] Frait Z and MacFadden H 1965 *Phys. Rev.* A **139** 1173
[10] Kaul S N and Siruguri V 1992 *J. Phys.: Condens. Matter* **4** 505
[11] Wohlfarth E P 1980 *Ferromagnetic Materials* ed E P Wohlfarth (New York: North-Holland) p 1
[12] Kanemaki S, Takehira O, Fukamichi K and Mizutani U 1989 *J. Phys.: Condens. Matter* **1** 5903
[13] Alperin H A, Steinsvoll O, Shirane G and Nathans R 1966 *J. Appl. Phys.* **37** 1052
[14] Sinclair R N and Brockhouse B R 1960 *Phys. Rev.* **120** 1638
[15] Janak J F 1978 *Solid State Commun.* **25** 53
[16] Edwards D M and Wohlfarth E P 1968 *Proc. R. Soc.* A **303** 127
[17] Hasegawa H 1979 *J. Phys. Soc. Japan* **46** 1504; 1981 *Electron Correlation and Magnetism in Narrow-Band Systems (Springer Series in Solid-State Sciences 29)* ed T Moriya (Berlin: Springer) p 38
[18] Hubbard J 1979 *Phys. Rev.* B **19** 2626; 1979 *Phys. Rev.* B **20** 4584; 1981 *Electron Correlation and Magnetism in Narrow-Band Systems (Springer Series in Solid-State Sciences 29)* ed T Moriya (Berlin: Springer) p 29
[19] Moriya T 1979 *J. Magn. Magn. Mater.* **14** 1; 1983 *J. Magn. Magn. Mater.* **31–4** 10 and references therein; 1985 *Spin Fluctuations in Itinerant Electron Magnetism (Springer Series in Solid-State Sciences 56)* (Berlin: Springer)
[20] Lonzarich G G and Taillefer L 1985 *J. Phys. C: Solid State Phys.* **18** 4339
[21] Mishra S G 1990 *Mod. Phys. Lett.* B **4** 83
[22] Hirsch J E 1991 *Phys. Rev.* B **44** 675 and references therein
[23] Takeuchi J and Masuda Y 1979 *J. Phys. Soc. Japan* **46** 468
[24] Tange H, Inoue K and Shirakawa K 1986 *J. Magn. Magn. Mater.* **54–7** 303
[25] Kakehashi Y 1990 *J. Magn. Magn. Mater.* **90–1** 333; 1991 *Phys. Rev.* B **43** 10 820
[26] Greig D, Gallagher B L, Howson M A, Law D S L, Norman D and Quinn F M 1988 *Mater. Sci. Eng.* **99** 265
[27] Singal C M and Das T P 1977 *Phys. Rev.* B **16** 5068
[28] Janak J F 1977 *Phys. Rev.* B **16** 255
[29] Moruzzi V L, Janak J F and Williams A R 1978 *Calculated Electronic Properties of Metals* (New York: Pergamon)
[30] Oelhafen P 1983 *Glassy Metals II* ed H Beck and H J Güntherodt (New York: Springer) p 283
[31] Obi Y, Wang L C, Motsay R and Onn D G 1982 *J. Appl. Phys.* **53** 2304
[32] Chen H S, Aust K T and Waseda Y 1981 *J. Non-Cryst. Solids* **46** 307
[33] Iskhakov R S, Brushtumov M M and Chekamov A S 1987 *Fiz. Tverd. Tela* **29** 2699 (1987 *Sov. Phys.–Solid State* **29** 1553) and references therein
[34] Kaul S N and Rosenberg M 1982 *Phys. Rev.* B **25** 5863